

The XYZ chain with Dzyaloshinsky-Moriya interactions: from spin-orbit-coupled lattice bosons to interacting Kitaev chains

Sebastiano Peotta⁽¹⁾, Leonardo Mazza⁽²⁾, Ettore Vicari⁽³⁾,
Marco Polini⁽⁴⁾, Rosario Fazio^(2,5), and Davide Rossini⁽²⁾

(1) Department of Physics, University of California, San Diego, La Jolla, CA 92093, USA

(2) NEST, Scuola Normale Superiore and Istituto Nanoscienze-CNR, I-56126 Pisa, Italy

(3) Dipartimento di Fisica dell'Università di Pisa and INFN, Largo Pontecorvo 3, I-56127 Pisa, Italy

(4) NEST, Istituto Nanoscienze-CNR and Scuola Normale Superiore, I-56126 Pisa

(5) Center for Quantum Technologies, National University of Singapore, Singapore

Abstract. Using the density-matrix renormalization-group algorithm (DMRG) and a finite-size scaling analysis, we study the properties of the one-dimensional completely-anisotropic spin-1/2 XYZ model with Dzyaloshinsky-Moriya (DM) interactions. The model shows a rich phase diagram: depending on the value of the coupling constants, the system can display different kinds of ferromagnetic order and Luttinger-liquid behavior. Transitions from ferromagnetic to Luttinger-liquid phases are first order. We thoroughly discuss the transition between different ferromagnetic phases, which, in the absence of DM interactions, belongs to the XX universality class. We provide evidence that the DM exchange term turns out to split this critical line into two separated Ising-like transitions and that in between a disordered phase may appear. Our study sheds light on the general problem of strongly-interacting spin-orbit-coupled bosonic gases trapped in an optical lattice and can be used to characterize the topological properties of superconducting nanowires in the presence of an imposed supercurrent and of interactions.

PACS numbers: 03.75.Mn, 05.30.Rt, 75.10.Pq, 71.70.Ej

1. Introduction

Ultracold atoms in optical lattices constitute a unique tool to study equilibrium as well as non-equilibrium properties of many-body quantum systems. The versatility of these setups, offered by the possibility of manipulating and initializing them in a wide range of regimes for several choices of atomic species, has led to an impressive number of breakthroughs in the study of strongly correlated systems of bosons and fermions, as well as of their mixtures [1, 2]. By dressing atomic states with properly-designed laser fields it is possible to engineer synthetic gauge fields [3, 4], thus paving the way for the exploration of Bose-Einstein condensates (BEC) and degenerate Fermi gases in presence of external magnetic fields [5] and spin-orbit coupling [6, 7, 8], even in the presence of optical lattices [9, 10, 11, 12, 13].

In particular, the experimental realization of a spin-orbit-coupled (SOC) BEC [6] has brought to the attention of the community the problem of investigating the interplay between interactions and non-Abelian gauge fields. In the Abelian case (i.e. for an external magnetic field), this interplay leads to the spectacular physics of the fractional quantum Hall effect [14]. In the case of weak interactions, the theoretical characterization has been thorough and detailed [15]. However, ultracold bosonic atoms can be driven into the strongly-interacting regime by means of an optical lattice, and for deep enough potentials a transition to a Mott insulating phase takes place [1, 2]. Whereas the density distribution of the cold atom gas in a Mott insulating phase is constrained to yield an integer number of particles per site, multi-component bosonic gases can display a variety of possible phases due to the underlying pseudo-spin degrees of freedom. For example, different types of “magnetic” orderings, both in the insulating and superfluid regimes, can occur [1].

So far only two- and three-dimensional lattice systems have been investigated (see for example [16, 17, 18, 19, 20, 21, 22, 23, 24, 25] and references therein) and the phase diagram has been shown to feature several intriguing properties. The superfluid phase can display exotic features and it can be spatially modulated, whereas in the Mott insulator (MI) phase the bosonic Hamiltonian can be mapped [17] onto an XYZ-model with Dzyaloshinsky-Moriya (DM) interactions [26, 27]. The phase diagram of this model in one spatial dimension (1D) has not been completely mapped out till now. In this Article we address this problem by means of a Density-Matrix Renormalization-Group (DMRG) algorithm [28, 29]. The main results of this analysis are presented in Fig. 1. The implications of these results on the magnetic phases of SOC bosonic MIs are discussed.

Remarkably, this study sheds light also on the topological properties of 1D nanowires [30, 31]. As first pointed out by Kitaev [32], 1D fermionic systems undergo a topological phase transition in the presence of p-wave pairing. The topological phase is characterized by the presence of zero-energy Majorana modes localized at the end points of the chain. Using our results, we are able to discuss the robustness of such edge modes to the simultaneous presence of interactions and of an external magnetic field,

which couples to the fermionic motional degrees of freedom. This study widens previous analysis on interacting Kitaev wires [33, 34, 35, 36].

Our Article is organized as follows. In Section 2 we introduce our model, i.e. the spin-1/2 Hamiltonian of the XYZ model with DM interactions. We highlight its connections to the mentioned bosonic and fermionic models. The main DMRG results concerning the characterization of the phase diagram are reported in Section 3 and are supplemented by the appropriate finite-size scaling analysis. In Section 4 we discuss these results from the point of view of lattice bosons and spinless fermions mentioned above. We conclude our work with Section 5, where a summary of our results is presented together with an outlook on future investigations.

2. The Model

We study the XYZ spin-1/2 Hamiltonian with a DM interaction term ($\hbar = 1$) [26, 27]:

$$\hat{\mathcal{H}} = \hat{\mathcal{H}}_{\perp} + \hat{\mathcal{H}}_z, \quad (1)$$

where

$$\hat{\mathcal{H}}_{\perp} = - \sum_j \left(J e^{i\varphi} \hat{S}_j^+ \hat{S}_{j+1}^- + J_{\Delta} \hat{S}_j^+ \hat{S}_{j+1}^+ \right) + \text{H.c.}, \quad (2)$$

$$\hat{\mathcal{H}}_z = J_z \sum_j \hat{S}_j^z \hat{S}_{j+1}^z. \quad (3)$$

Here $J > 0$ and \hat{S}_j^{α} ($\alpha = x, y, z$) are spin-1/2 operators on the j -th site (\hat{S}_j^{\pm} are the corresponding raising/lowering operators). The Hamiltonian contains short-range interactions characterized by three coupling constants: $J e^{-i\varphi}$, J_{Δ} , and J_z . Because of the term controlled by J_{Δ} , which is here taken to be a real number, the phase φ cannot be gauged away even in an open chain and is related to a DM interaction. Indeed, by expressing Hamiltonian (2) in terms of \hat{S}_i^x and \hat{S}_i^y , one gets $\hat{\mathcal{H}}_{\perp} = - \sum_i \left(J_x \hat{S}_i^x \hat{S}_{i+1}^x + J_y \hat{S}_i^y \hat{S}_{i+1}^y + D \hat{\mathbf{z}} \cdot \hat{\mathbf{S}}_i \times \hat{\mathbf{S}}_{i+1} \right)$ with the identification $J e^{i\varphi} = (J_x + J_y + i2D)/4$ and $J_{\Delta} = (J_x - J_y)/4$. In the rest of the Article we discuss the zero-temperature phase diagram of the Hamiltonian (1) using the parametrization given in Eqs. (2) and (3).

2.1. Related Models: Spin-Orbit-Coupled Lattice Bosons and Fermionic Nanowires

As anticipated in the Introduction, the model defined in Eq. (1) is related to two paradigmatic cold-atom and condensed-matter models. It is useful at this stage to make these mappings explicit, although already known in the literature, so that our findings can be compared more easily with related bibliography.

The Hamiltonian (1) represents an effective model for a lattice system loaded with two bosonic species (i.e. a hyperfine doublet in the context of ultracold atoms) with an

anisotropic interaction and spin-orbit coupling. The corresponding 1D Bose-Hubbard (BH) Hamiltonian reads:

$$\hat{\mathcal{H}}_{\text{BH}} = \sum_j \left[-t \left(\hat{b}_j^\dagger e^{i\alpha\tau^y} \hat{b}_{j+1} + \text{H.c.} \right) + \frac{g_1}{2} (\hat{n}_j)^2 + \frac{g_2}{2} \left(\sum_{\beta,\gamma} \hat{b}_{j,\beta}^\dagger \tau_{\beta,\gamma}^z \hat{b}_{j,\gamma} \right)^2 \right]. \quad (4)$$

Here $\hat{b}_j = (\hat{b}_{j,\uparrow}, \hat{b}_{j,\downarrow})$ is a bosonic annihilation operator for the two components at site j , which are for brevity addressed with the pseudo-spin $\{\uparrow, \downarrow\}$ notation; \hat{n}_j is the on-site density operator and τ^β are the Pauli matrices which act on the pseudo-spin degrees of freedom ($\tau_{\beta,\gamma}^z$ denotes the matrix elements of τ^z). The first term in Eq. (4) represents the hopping, whose amplitude is t ; the angle $\alpha \neq 2\pi m$, $m \in \mathbb{Z}$, quantifies the strength of spin-orbit coupling (in the continuum limit the momentum operator would couple to the y -component of the spin). The last two terms describe interactions between bosons: the term proportional to g_1 is the standard BH repulsive term, while the one controlled by g_2 fixes a preferred orientation in spin space.

Note that we have chosen two orthogonal preferred directions for the spin-orbit coupling and interaction anisotropy, thereby fully breaking the SU(2) spin symmetry. The choice of a spin-orbit axis aligned along z produces a less interesting model, as the corresponding spin-orbit term can be gauged away in an open chain. If $g_1 \gg |g_2|$ and one is well inside the MI phase, only spin degrees of freedom play a role. In this limit it is therefore convenient to introduce an effective spin Hamiltonian. A straightforward second-order expansion in the small parameter t/g_1 yields a model which is formally equivalent to the one in Eq. (1), modulo a different labeling of the axes. Introducing the shorthand $g \equiv g_2/g_1$, the parameters of the two models are related by the following identities:

$$\begin{aligned} J_z &= -\frac{4t^2}{g_1} \frac{1}{1-g}, \\ J e^{i\varphi} &= \frac{4t^2}{g_1} \frac{1}{1-g} \frac{1-g}{2(1+g)} e^{i2\alpha}, \\ J_\Delta &= -\frac{4t^2}{g_1} \frac{\cos(2\alpha)}{1-g} \frac{g}{1+g}. \end{aligned} \quad (5)$$

The most relevant effect of spin-orbit coupling is to introduce a DM interaction [17, 18]. Thus, the phase diagram that we are going to present is relevant for future experiments with synthetic gauge fields in 1D optical lattices loaded with two bosonic species.

Interestingly, studying the Hamiltonian (1) is also important for the problem of interacting topological insulators and, more specifically, for the robustness of zero-energy Majorana modes in semiconducting nanowires [30, 31, 32]. By means of a Jordan-Wigner transformation, the Hamiltonian (1) can be mapped onto a 1D model of interacting spinless fermions with hopping amplitude $J e^{-i\varphi}$, p-wave pairing potential J_Δ and a nearest-neighbor interaction J_z :

$$\hat{\mathcal{H}}_{\text{K}} = \sum_j \left[- (J e^{i\varphi} \hat{c}_j^\dagger \hat{c}_{j+1} + J_\Delta \hat{c}_j \hat{c}_{j+1} + \text{H.c.}) + J_z \left(\hat{m}_j - \frac{1}{2} \right) \left(\hat{m}_{j+1} - \frac{1}{2} \right) \right]. \quad (6)$$

Here \hat{c}_j annihilates a fermion at site j and $\hat{n}_j \equiv \hat{c}_j^\dagger \hat{c}_j$ is the usual density operator. The complex phase φ represents the coupling to an external magnetic field, which induces a finite supercurrent into the system. The interplay of this term with nearest-neighbor interactions has not been fully investigated yet.

2.2. Exactly Solvable Cases

In this Section we present some properties of the XYZ-model (1) that hold for special properties of the microscopic couplings, where an exact solution is available.

2.2.1. $\varphi = 0$ and $\varphi = \pi$. — It is useful to recall what happens to the XYZ-model (1) when $\varphi = 0$. In this case an exact solution is known [37, 38]. In the thermodynamic limit the system spontaneously breaks the \mathbb{Z}_2 symmetry along the axis with the largest value of $|J_\alpha|$ ($\alpha = x, y, z$). For $J_\alpha > 0$ there is ferromagnetic order, while $J_\alpha < 0$ yields antiferromagnetic (Néel) order. The system is critical whenever there are two couplings that are equal and their absolute value exceeds that of the third one; in that case a Luttinger liquid (LL) phase appears. Considering the $(J_\Delta/J, J_z/J)$ plane, in the spirit of the parametrization of Eq. (2), the XYZ model is thus critical for $J_\Delta = 0, |J_z| \leq 2J$ (the equality corresponds to the ferromagnetic and antiferromagnetic Heisenberg models), and for $J_\Delta = \pm(|J_z|/2 - J)$ for $|J_z| \geq 2J$.

The case $\varphi = \pi$ is completely equivalent, since a unitary rotation connects the model for $\{J, J_\Delta, J_z, \varphi = \pi\}$ with $\{J, -J_\Delta, J_z, \varphi = 0\}$.

2.2.2. $\varphi \neq 0, \pi; J_z = 0$. — The most relevant exactly solvable case for $\varphi \neq 0, \pi$ is the case $J_z = 0$. As highlighted by Eq. (6), the model (1) can be mapped into a free fermion model and is thus exactly solvable [39, 40, 41]. The system is gapless for $|J_\Delta/J| \leq |\sin \varphi|$. The most important effect of the DM interaction is thus to extend the critical line appearing for $J_\Delta = 0$ to a region of finite width.

2.2.3. $\varphi \neq 0, \pi; J_\Delta = 0$. — Interestingly, also the case $J_\Delta = 0$ yields an exactly solvable model [42]. In this case a unitary transformation can be used to gauge away the quantity φ , so that Eq. (1) reduces to the well-known XXZ model. The system is gapless for $|J_z/J| \leq 2$ and displays power-law decaying correlations, which are typical of a LL. However, because of the rotation needed to gauge away φ , correlations are twisted into the x - y plane.

2.2.4. Symmetries. — When $\varphi \neq 0$ the number of symmetries of the system is relatively small; nonetheless there are a few ones which yield important information.

- (i) Rotation of $\pi/2$ in the $x - y$ plane: $\hat{S}_j^x \rightarrow \hat{S}_j^y; \hat{S}_j^y \rightarrow -\hat{S}_j^x; \hat{S}_j^z \rightarrow \hat{S}_j^z$. This unitary transformation changes $J_\Delta \rightarrow -J_\Delta$, leaving the other coupling constants unchanged. The sign of J_Δ is therefore unessential.

- (ii) Inversion with respect to the center of the chain: $\hat{S}_j^\alpha \rightarrow \hat{S}_{L-j}^\alpha$. This unitary transformation changes $Je^{-i\varphi} \rightarrow Je^{i\varphi}$, leaving the other coupling constants unchanged. The sign of φ is therefore unessential.
- (iii) Rotation of π in the x - y plane, only at even sites [43]: $\hat{S}_j^x \rightarrow -\hat{S}_j^x$; $\hat{S}_j^y \rightarrow -\hat{S}_j^y$; $\hat{S}_j^z \rightarrow \hat{S}_j^z$ for j even. This unitary transformation changes $Je^{-i\varphi} \rightarrow Je^{-i(\varphi+\pi)}$ and $J_\Delta \rightarrow -J_\Delta$, leaving the other coupling constants unchanged. Together with the previous symmetry, it implies that the phase φ can be taken in the interval $[0, \pi/2]$.

3. Phase diagram

We now present the main results of this Article, i.e. the zero-temperature phase diagram of the XYZ-model with DM interactions (1), obtained via a DMRG study. Our numerical simulations were performed for systems with open boundary conditions up to $L = 400$ sites, keeping at most $m = 120$ states. We checked that the location of the phase boundaries is not affected by the value of the cut-off m . We focus only on the ferromagnetic region of the phase diagram centered around $J_z/J \sim -2$ because this is the most relevant case for bosons in optical lattices (see Section 2.1). Without loss of generality, we take $J_\Delta/J \geq 0$.

The phase diagram of (1) is shown in Fig. 1 for $\varphi = 1$. The study of other values of φ resulted only in quantitative differences. The most relevant quantum phases are those which characterize the model also for $\varphi = 0$, namely, two ferromagnetic phases with different orientation (along the z and x axes) and a LL region. As already discussed, the DM interaction is responsible for the finite width of the gapless region; furthermore, it rigidly shifts the transition between the two ferromagnetic phases (the case $\varphi = 0$ is plotted in Fig. 1 with a dashed line). One of the most interesting features of this phase diagram is the absence of a direct transition between the ferromagnetic phases, where a new intermediate disordered region appears (white area in Fig. 1). As we will discuss below, the LL-to-ferromagnet transitions are first order, whereas according to our analysis a self-consistent description in terms of two Ising-like critical lines can be formulated for the transition between the ferromagnetic phases. All the different phases seem to converge in a region that could not be reliably analyzed because of accuracy problems while dealing with sizes $L > 400$ (see Appendix A); the existence or absence of a triple point could not be assessed. We now analyze the different transitions in more details; data will be presented for parameters running along the blue segments in Fig. 1.

3.1. Phase Transition between a Ferromagnetic Phase and a Luttinger-Liquid

Let us first consider the transition between the LL and the ferromagnetic phases, cuts “1” and “2”. Ferromagnetically ordered phases can be distinguished either by measuring the magnetization $M_\alpha \equiv \sum_i \langle \hat{S}_i^\alpha \rangle / L$ ($\alpha = x, y, z$), or by analyzing the asymptotic behavior of correlation functions. We show results based on the former indicator: no significant advantages were noticed by computing correlation functions. For a finite

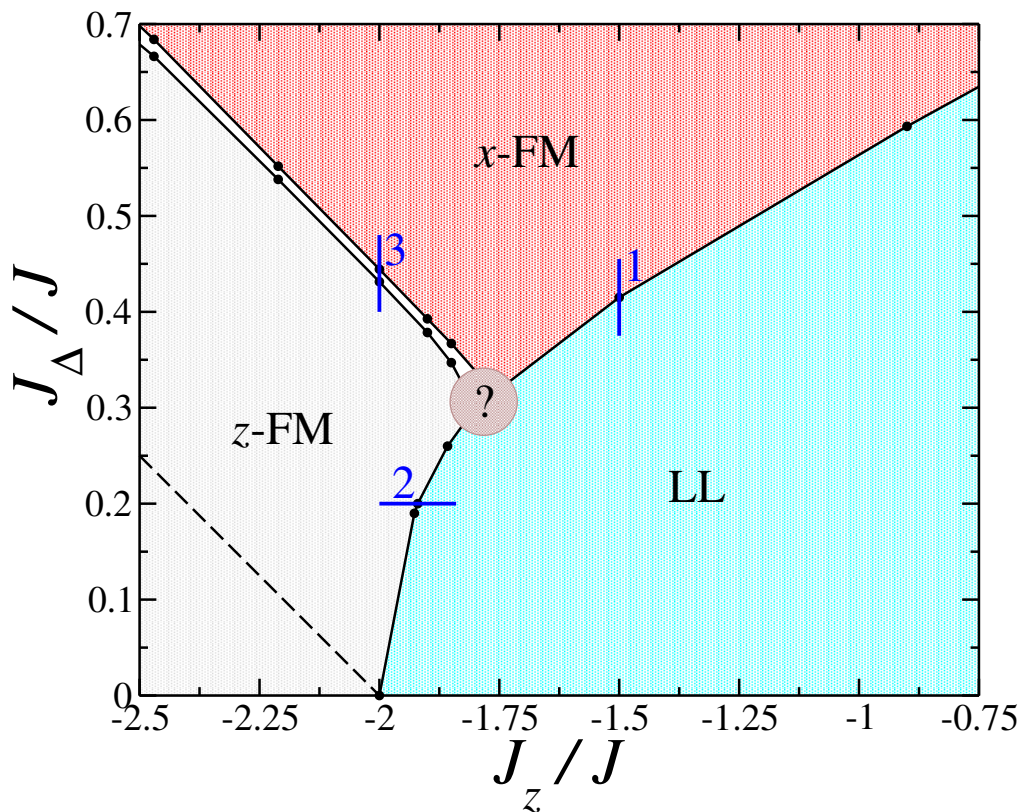


Figure 1. (color online). Zero-temperature phase diagram of the XYZ model with DM interaction as defined by Hamiltonian (1) for $\varphi = 1$. Different colors denote the various phases: The critical Luttinger liquid (LL) phase is depicted in blue, while the two ferromagnets (x -FM and z -FM) are in red and in gray, respectively. The circle with a question mark identifies a region which could not be reliably investigated and that may host a triple point. The dashed line denotes the transition between the two ferromagnetic phases occurring at $\varphi = 0$. The analysis of our numerical data supports the existence of an intermediate disordered (white) region separating the two ferromagnetic ones. Straight blue segments indicate the three cuts along which the various phase transitions are specifically addressed in the text.

chain of length L , spontaneous symmetry breaking is forbidden: the two lowest-energy states are non-magnetic and their degeneracy decreases exponentially with system size. However, already for $L \sim 100$ the degeneracy is far too small to be resolved by DMRG simulations. To avoid numerical complications, in the study of the ferromagnetic – LL phase boundary we break the symmetry by adding two small magnetic fields $\mu_B B_{\text{edge}} \approx 10^{-5} J$ acting on the spins at the end points of the chain. (We have checked that our results do not depend on the value of such fields). In Figs. 2 and 3 we show the magnetization of the system across the cuts “1” and “2”, respectively. Our data clearly display ferromagnetic order as a function of J_Δ or as a function of J_z . A finite magnetization appears above a critical value of J_Δ (x -direction) and below a critical value of J_z (z -direction). The phase transition between the LL phase and any of the two ferromagnetic phases is of the first order: this is signaled by a discontinuity both in

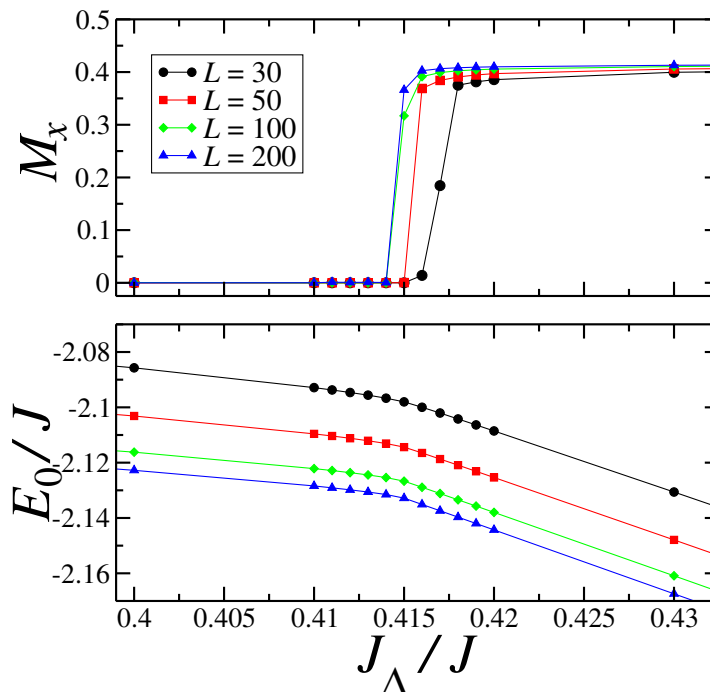


Figure 2. (color online). Study of the LL - ferromagnet transition along cut “1” ($J_z/J = -1.5$) in the phase diagram in Fig. 1. Upper panel: magnetization along x as a function of J_Δ/J . Different symbols and colors denote data for various system sizes. A discontinuity in M_x signaling a first-order transition is observed at $(J_\Delta/J)_c \sim 0.415$. Lower panel: ground-state energy (in units of j and per site) as a function of J_Δ/J . The discontinuity in its first derivative locates the transition point and the result is in agreement with the magnetization data.

the magnetization and in the first derivative of the ground-state energy.

Regarding the gapless phase, we can certainly conclude that no ferromagnetic order is present, even if we did not make detailed simulations to analyze its properties. The blue region in Fig. 1 can be confidently classified as an extension of the gapless LL phase of the XXZ model (at $J_\Delta = 0$), as it can be shown in a perturbative approach with respect to J_Δ .

3.2. Phase Transition between Two Ferromagnetic Phases

We now investigate the phase diagram between the two ferromagnetic phases, denoted by x -FM and z -FM in Fig. 1. In the pure XYZ chain, the disappearance of one kind of order (for instance along z) coincides with the appearance of another kind of order (for instance along x). It is a continuous phase transition of the XX universality class, akin to that present in the XY chain, which is enforced by the symmetries of the model.

Such symmetries are lost in the presence of a DM interactions, i.e., when $\varphi \neq 0$. In order to investigate their effects we present a finite-size scaling of the ratios [44] $R_\alpha = \xi_\alpha/L$, where ξ_α is the correlation length for the $\alpha = x, z$ component of the spin

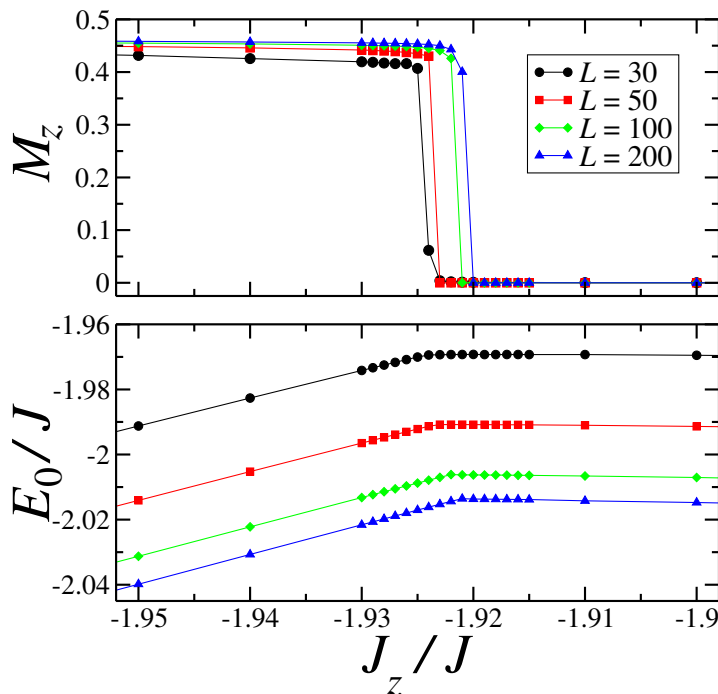


Figure 3. (color online). Study of the LL - ferromagnet transition along cut “2” ($J_\Delta/J = 0.2$) in the phase diagram in Fig. 1. Upper panel: magnetization along z as a function of J_z/J . A discontinuity in M_z signaling a first-order transition is observed at $(J_z/J)_c \sim -1.922$. Lower panel: ground-state energy (in units of J and per site) as a function of J_z/J . The discontinuity in its first derivative locates the transition point and is in agreement with the magnetization data.

variables, i.e.,

$$\xi_\alpha = \sqrt{\frac{\sum_r r^2 \langle \hat{S}_i^\alpha \hat{S}_{i+r}^\alpha \rangle}{2 \sum_r \langle \hat{S}_i^\alpha \hat{S}_{i+r}^\alpha \rangle}}; \quad i = L/2. \quad (7)$$

These quantities are particularly useful to identify continuous transitions characterized by diverging length scales for the correlation functions $\langle S_i^\alpha S_{i+r}^\alpha \rangle$. Indeed around such critical points and for large enough L , they are expected to behave as [45, 46],

$$R_\alpha = f(\delta_\alpha \cdot L^{1/\nu}) + \dots \quad (8)$$

where $\delta_\alpha \equiv J_\Delta/J - (J_\Delta/J)_{c,\alpha}$ controls the distance from the critical point, and ν is the length-scale critical exponent. The dots indicate scaling corrections which are generally suppressed by powers of the inverse size [44]. Therefore, as implied by Eq. (8), the presence of a crossing point among data sets for different sizes L provides the evidence of a critical point. The slope at the crossing point is controlled by the universal exponent ν associated with the universality class of the transition.

To begin with, we show results at $\varphi = 0$, i.e. for the plain XYZ model, at $J_z/J = -3$. In this case we expect a single transition point at $J_\Delta/J = 1/2$ between ferromagnetic phases along x and z ; at the transition point one must recover the

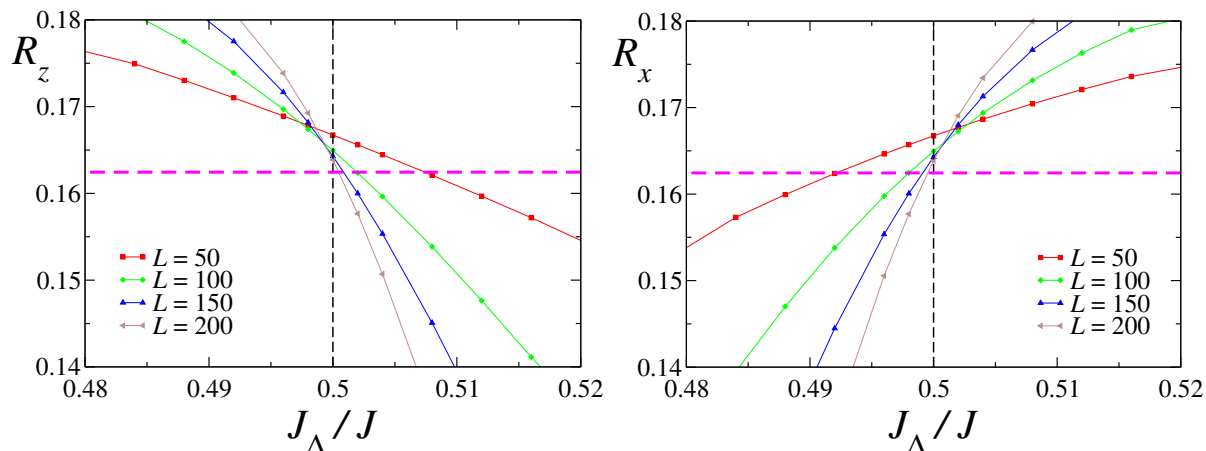


Figure 4. (color online). Finite-size scaling study of the transition between the two ferromagnetic phases in the case $\varphi = 0$. $R_z = \xi_z/L$ (left) and $R_x = \xi_x/L$ (right) are plotted as functions of the couplings J_Δ/J for $J_z = -3J$. Curves corresponding to different system sizes cross at the critical point, which is unique and exactly known, $(J_\Delta/J)_c = 1/2$. The dashed line shows the predicted value of $R^* = 0.162445\dots$ in the $L \rightarrow \infty$ limit.

critical properties of the XXZ model. In Fig. 4 we plot the quantities R_x and R_z . Both of them clearly show a crossing point, which approach the same critical point as expected. Moreover, at the crossing point the values of R_x and R_z approach the value $R_x^* = R_z^* = 0.162445\dots$, as predicted by computations using conformal field theory.

We now move to the case $\varphi \neq 0$, for which no symmetry forces the XXZ universality class, and thus the nature of the transition between the two ferromagnetic phases may drastically change. We focus in particular on the behavior along the “cut 3” of the phase diagram in Fig. 1, along which $J_z/J = -2$. We present DMRG results up to $L = 400$, see Appendix A for technical details on the accuracy of the method.

Figs. 5 and 6 show results for the ratios R_α , see Eq. (7), and the susceptibility-like quantities

$$W_\alpha \equiv \frac{1}{L} \sqrt{\left\langle \left(\sum_i \hat{S}_i^\alpha \right)^2 \right\rangle}, \quad (9)$$

respectively. These quantities do not show abrupt changes which may hint at first-order transitions, like those appearing in Fig. 2. Therefore, we are lead to exclude first-order transitions between the x -FM and z -FM phases.

Within the scenario based on continuous phase transitions, two possibilities can be envisioned: (i) the transition splits into two separated critical lines, (ii) the transition remains unique. For the case (i), two subcases are possible: (ia) the region in-between possesses both magnetic orders along x and z , (ib) the region in-between does not possess any magnetic order along x or z .

The results in Fig. 5 suggest two distinct transitions. Indeed their data sets for different L appear to cluster at different points, i.e. $J_\Delta/J \approx 0.435$ for R_z and $J_\Delta/L \approx 0.440$ for R_x . Between these two crossing points the data clearly decrease with

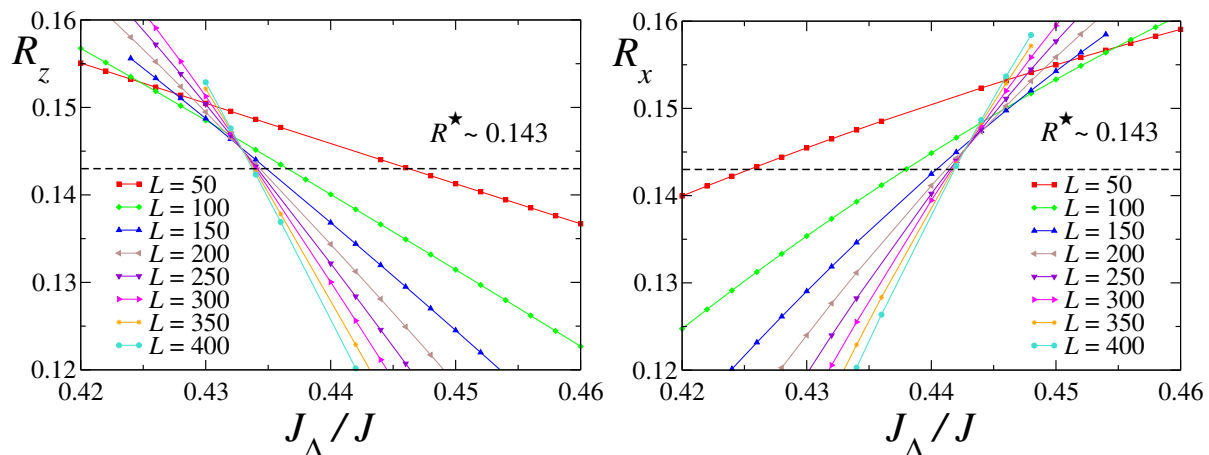


Figure 5. (color online). Finite-size scaling study of the transition between the two ferromagnetic phases in Fig. 1 along cut “3”. The functions $R_z = \xi_z/L$ (left) and $R_x = \xi_x/L$ (right) defined in the main text are plotted as functions of the couplings J_Δ/J for $J_z = -2J$. Curves for different system sizes show the appearance of a crossing point, and the plots seem to suggest that there are two distinct ones.

increasing L , thus suggesting a disordered phase for both x and z order parameters. This behavior seems to exclude the presence of a ordered phase with both x and z magnetic order.

Within the scenario of two transitions, with an intermediate disordered phase for both x and z magnetic variables, a natural hypothesis is that the two distinct transitions belong to the two-dimensional (2D) Ising universality class, with \mathbb{Z}_2 -like order parameters related to expectation values of the spin operators S_i^x and S_i^z . We recall that the critical exponent of the 2D Ising universality class are $\nu = 1$ (length-scale exponent) and $\eta = 1/4$ (related to the behavior of the two-point function at criticality). In order to check this scenario we perform a finite-size scaling analysis of the data. Assuming a transition in the 2D Ising universality class, we expect that

$$R_\alpha(J_\Delta/J, L) \approx \mathcal{R}(\delta L); \quad (10)$$

where $\delta \equiv J_\Delta/J - (J_\Delta/J)_{\alpha,c}$ and $\mathcal{R}(w)$ is a universal function (apart from a trivial normalization of the argument), generally depending on the boundary conditions. Corrections to the above scaling behavior are suppressed by powers of $1/L$, in particular the leading ones are [44] $O(L^{-3/4})$. In order to determine the critical values of J_Δ/J for the two transitions, we fit the data around the crossing point using the simple ansatz

$$R_\alpha(J_\Delta/J, L) = R^* + c \delta_\alpha L, \quad (11)$$

where we keep only the first order of the expansion of the r.h.s. of Eq. (10), which should provide a good approximation sufficiently close to the crossing point. The data in the fit are selected using self-consistent scaling conditions with increasing L [47]: we select those satisfying $-\varepsilon_1 < R_\alpha/R^* - 1 \lesssim \varepsilon_2$ with $\varepsilon_1 \ll \varepsilon_2 \approx 0.1$ (the asymmetry between $\varepsilon_{1,2}$ is essentially due to the fact that the data in the ordered phase are expected to be less contaminated by the other degrees of freedom). The fit neglects the $O(L^{-3/4})$

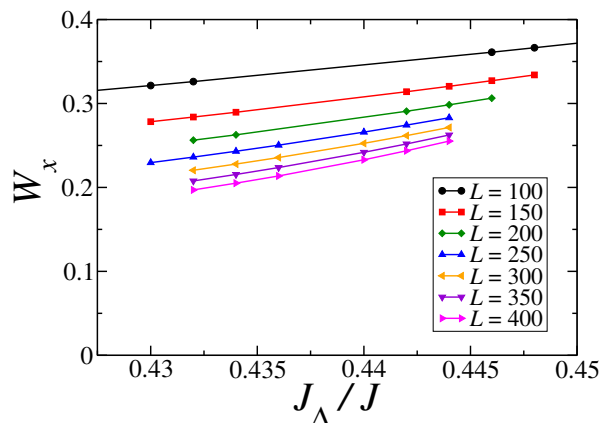


Figure 6. (color online). The squared magnetization W_x as a function of J_Δ/J for $J_z/J = -2$ (cut “3”) for several system lengths L .

corrections. Their effect is kept under control by checking the stability of the fit results for different values of L_{\min} , which is the minimum system size we have considered. This numerical analysis shows that the data are consistent with the hypothesis of two Ising transitions, yielding the estimates

$$(J_\Delta/J)_{x,c} = 0.441(2), \quad R_x^* = 0.143(2), \quad (12)$$

and

$$(J_\Delta/J)_{z,c} = 0.435(2), \quad R_z^* = 0.143(2), \quad (13)$$

where the errors are such to take into account the variation of the results varying L_{\min} . In the fits we take also into account the precision of the data, which is estimated to be roughly $\Delta R \approx 2 \times 10^{-5}(L/200)^5$, see [Appendix A](#). The quality of this analysis is demonstrated by [Fig. 7](#), where the data of R_x versus the scaling variable $\delta_x L$ (with $\delta_x = J_\Delta/J - 0.441$) show a good collapse with increasing L . Analogous results are obtained for R_z at the other transition.

As a further check of this scenario, in [Fig. 7](#) we plot the crossing points of the data of R_x and R_z for different chain lengths. General finite-size scaling arguments predict that they must converge to the critical point. In the case of the Ising universality class, the renormalization-group analysis of [Ref. \[44\]](#) predicts that the crossing points of the ratio R_α must converge to the critical point with $O(L^{-7/4})$ corrections. The data in [Fig. 7](#) nicely support this behavior. They appear to extrapolate to two different critical points, in agreement with the estimates reported in [Eqs. \(12\) and \(13\)](#).

However, we should also mention an apparent contradiction with the hypothesis of Ising transitions. For the Ising universality class with open boundary conditions the value of R^* can be computed exactly [\[44\]](#), obtaining $R^* = 0.159622\dots$. But this is not compatible with the estimates of R_x^* and R_z^* , cf. [Eqs. \(12\) and \(13\)](#). We ascribe this inconsistency to the residual effects of the DM interactions, which may somehow induce nontrivial effective boundary conditions for the Ising critical modes, and thus be responsible for the mentioned discrepancy.

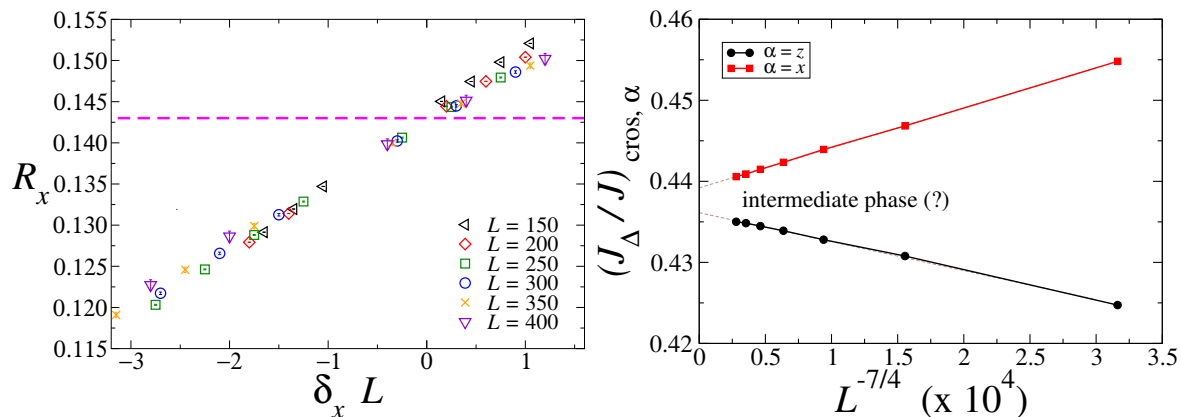


Figure 7. (color online). Left: The quantity R_x is plotted as a function of $\delta_x \cdot L$, using the fitted value (12) for $(J_\Delta/J)_{c,x}$. We display only data for L in the interval $150 \leq L \leq 400$, for the most accurate DMRG simulations with $m = 100$ states. Error bars, estimated as $\Delta R \approx 2 \cdot 10^{-5}(L/200)^5$, are shown (and are of the order or less of the marker size). The dashed line indicates the estimated value $R_x^* = 0.143(2)$. An analogous plot is obtained for $\alpha = z$. Right: Crossings points $(J_\Delta/J)_{\text{cross}, \alpha, L}$ of the $R_\alpha(J_\Delta/J)$ curves for lengths L and $L + 50$; the cut “3”, $J_z/J = -2$, is considered. The scaling behavior $L^{-7/4}$ is highlighted and upon extrapolation for $L \rightarrow \infty$ (thin dashed line) corroborates the possibility that an intermediate phase appears.

Concluding, these analyses provide evidence of the presence of a new disordered phase in a narrow region of the phase diagram between the x -FM and z -FM phases, see Fig. 1. The critical behaviors at the two transitions appear overall consistent with two Ising transitions. However, these results should not be considered as a conclusive analysis of the problem. Since the two transitions are very close, we cannot exclude that we are just observing a crossover, and that the two distinct crossing points will eventually converge towards a unique critical point for larger values of L , as in scenario (ii). In this respect, DMRG simulations for significantly larger system sizes are required to definitely exclude such a possibility. We have however presented strong evidence that this should not be the case.

4. Spin-Orbit-Coupled Bosons and Fermionic Nanowires

Finally, let us discuss the implications of the previous findings for the two specific models of bosons and fermions introduced in Section 2.1.

4.1. Bosons

We are interested in a strongly-interacting lattice model, and the system has been driven to a MI; we investigate its magnetic properties in the experimentally-relevant case of $g \sim 0$, $\alpha \in [0, \pi/4]$. The restriction on α descends from (i) the restriction on φ previously discussed, $\varphi \in [0, \pi/2]$, and (ii) Eqs. (5), which imply $\alpha = \varphi/2 + m\pi$, $m \in \mathbb{Z}$.

The case $g = 0$ is particularly simple, as it implies $J_\Delta = 0$ and $J_z = -2J$ independently of α . Thus, as discussed in Sec. 2.2, when the interaction is isotropic in spin space, the critical properties of the system are those of a ferromagnetic Heisenberg model. The independence of such properties on α is another way of stating that for isotropic interactions spin-orbit coupling can be gauged away.

For $g \neq 0$, the manipulation of Eqs. (5) shows that only a subregion of the plane $(J_z/J, J_\Delta/J)$ in Fig. 1 is accessible:

$$\frac{J_\Delta}{J} = \pm \frac{1}{2} \cos(\varphi) \left(\frac{J_z}{J} + 2 \right). \quad (14)$$

If we consider the case $\varphi = 1$ studied in Fig. 1, the system explores only the phase with ferromagnetic order along z and the LL phase. Extrapolating the fact that the disordered phase appears for every φ and maintains a slope $-1/2$ in the $(J_z/J, J_\Delta/J)$ plane, we conclude that a SOC bosonic MI cannot enter the ferromagnetic phase aligned along x for $J_z/J < -2$ and for any value of α . On the other hand, for $\varphi = 0$ the system is mapped onto a XZZ model and thus explores the phase with ferromagnetic order along x for $J_z/J > -2$ [48]. For continuity, this may extend to $\varphi \gtrsim 0$.

Let us finally mention the special value $\alpha = \pi/4$, for which $J_\Delta = 0$ and the system is mapped onto the XXZ model, which does not entail any ferromagnetic phase aligned along x . In particular, for this case:

$$\frac{J_z}{J} = -2 \frac{1+g}{1-g}, \quad e^{i\varphi} = i. \quad (15)$$

Thus, for $g \gtrsim 0$ the system enters a gapped ferromagnetic phase, whereas for $g \lesssim 0$ the phase is a critical LL.

4.2. Fermions

Let us now briefly comment on the implications of the phase diagram in Fig. 1 on the topological properties of the fermionic model in Eq. (6). The topological phase with Majorana edge modes corresponds to the ferromagnetic ordered phase oriented along x . In the absence of interactions, $J_z = 0$, a finite supercurrent $\varphi \neq 0$ diminishes its extension to the advantage of the gapless LL region, which thus cannot be topological. In the opposite case of strong attractive interactions, $J_z/J \rightarrow -\infty$, the model (6) corresponds to a simple model of attractive fermions without topological properties; we can thus conclude that the ferromagnetic phase along z is devoid of protected edge modes. Even if there is an appropriate Jordan-Wigner transformation that maps the z ferromagnetic spin phase to a fermionic system with Majorana modes, it does not coincide with the mapping used for deriving the Hamiltonian (6). From the phase diagram we can see that a finite attractive interaction increases the critical current that is required to destroy the topological phase. It is rather intriguing to investigate what may be the fermionic properties of the disordered phase appearing in between the ferromagnetic phases and to assess whether it is devoid of topological properties. We leave this analysis for future work.

5. Conclusions

In summary, we have analyzed the XYZ spin-1/2 chain in presence of Dzyaloshinsky-Moriya interactions. It presents a rich phase diagram, depicted in Fig. 1, which has been thoroughly studied in its ferromagnetic region, which is most relevant for spin-orbit-coupled bosonic gases loaded in 1D optical lattices. First-order quantum phase transitions separate gapless Luttinger-liquid phases from gapped ferromagnetic phases. Depending on the relative strength of the couplings, such ferromagnetic order can develop along different axes. The study of the direct phase transition between two ferromagnetic phases has proven to be particularly intriguing. Indeed, the Dzyaloshinsky-Moriya term breaks the symmetry that in the XYZ model forces that transition to be unique and of the XX universality class. Our investigation suggests that such critical line may split into two Ising-like phase transitions, which are characterized by means of a finite-size scaling analysis of the correlation length.

Our results are relevant for the characterization of the phase diagram of one-dimensional bosons in optical lattices in the presence of spin-orbit coupling and anisotropic spin interactions. Moreover, they allow the quantitative assessment of the stability of the topological phase of the Kitaev chain characterized by two zero-energy Majorana edge modes in presence both of interactions and of an external current. It is fascinating to speculate an extension of this study to ladder geometries, where additional degrees of freedom may give rise to new exotic phases [49].

During the completion of this manuscript we became aware of three works where one-dimensional lattice bosons with spin-orbit coupling are studied by means of density-matrix renormalization-group algorithms [50, 51, 52].

Acknowledgments

We thank P. Calabrese for fruitful discussions. This work was supported by the EU IP-SIQS (Grant agreement No 600645), and the Italian MIUR through PRIN (Project 2010LLKJBX) and through FIRB (Project RBFR12NLNA). L. M. is supported by Regione Toscana POR FSE 2007-2013. S. P. is supported by DOE under Grant No. DE-FG02-05ER46204.

Appendix A. Error Estimate for DMRG Data

The accuracy parameter for a DMRG calculation, which characterizes the outcome of the simulation, $|\Psi_{\text{DMRG}}\rangle$, is the so called “number of kept states m ”, that is the effective maximal Hilbert space dimension of each block [28, 29]. Such number indicates that its Schmidt decomposition entails at most m states. Clearly, the larger is m the better a target state $|\Psi\rangle$ can be approximated. In Fig. A1 we show the different values of R_z obtained for different values of m for a specific point of the phase diagram. In order to compute the error for the data at $m = 100$, which are used in the finite-size-

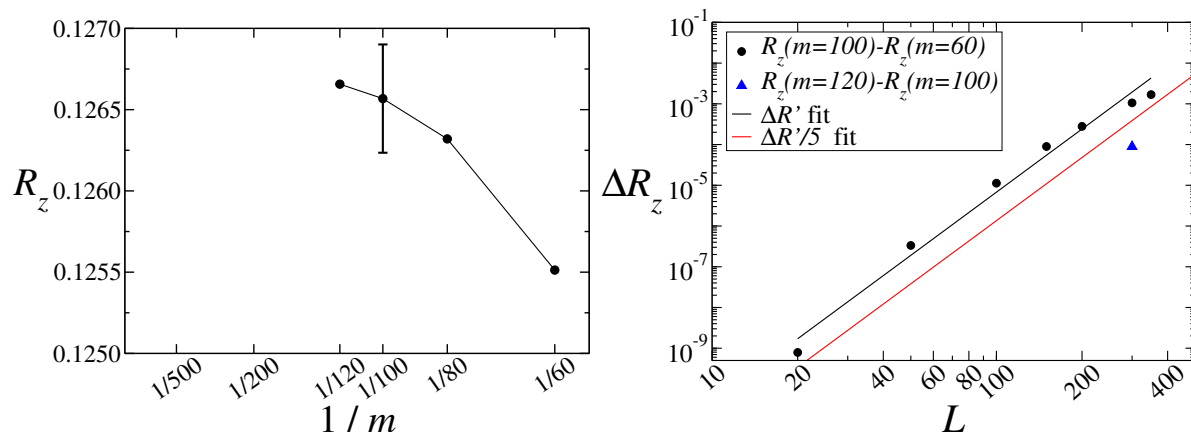


Figure A1. (color online). Accuracy of DMRG simulations for different values of m . (Left) R_z computed at $J_\Delta/J = 0.434$, $J_z/J = -2$, $\varphi = 1$ for a system of length $L = 300$. The number of kept states is 60, 80, 100 and 120; a clear convergence behavior appears. (Right) The error is estimated comparing outcomes for different m . The differences $R(m = 100) - R(m = 60)$ and $R(m = 120) - R(m = 100)$ are shown. The former is fitted by $\Delta R' = 10^{-4}(L/200)^5$. The error bars on the data at $m = 100$ are heuristically estimated considering $\Delta R \equiv \Delta R'/5$ (see also the bars in the left plot).

scaling in the text, we performed some simulations at $m = 120$, which were however computationally too demanding for a complete program of simulations (note also that the model does not conserve any magnetization, i.e. a symmetry that significantly lowers technical intricacies). It is possible to observe that $R(m = 120) - R(m = 100) \sim (R(m = 100) - R(m = 60))/5$. The error formula proposed in the text, $\Delta R \approx 2 \cdot 10^{-5}(L/200)^5$, is obtained via a fit of $R(m = 100) - R(m = 60)$ close to the quantum phase transition (see Fig. A1). A quantitative improvement of our finite-size-scaling analysis requires the study of significantly larger systems, for which numerical difficulties increase exponentially.

References

- [1] M. Lewenstein et al., *Adv. Phys.* **56**, 243 (2007).
- [2] I. Bloch, J. Dalibard, and W. Zwerger, *Rev. Mod. Phys.* **80**, 885 (2008).
- [3] J. Dalibard, F. Gerbier, G. Juzeliūnas, and P. Öhberg, *Rev. Mod. Phys.* **83**, 1523 (2011).
- [4] V. Galitski and I. B. Spielman, *Nature* **494** 1523 (2011).
- [5] Y.-J. Lin, R. L. Compton, K. J. Garcia, J. V. Porto and I. B. Spielman, *Nature* **462**, 628 (2009).
- [6] Y.-J. Lin, K. Jiménez-García, and I. B. Spielman, *Nature* **471**, 83 (2011).
- [7] L. W. Cheuk, A. T. Sommer, Z. Hadzibabic, T. Yefsah, W. S. Bakr, and M. W. Zwierlein, *Phys. Rev. Lett.* **109**, 095302 (2012).
- [8] P. Wang et al., *Phys. Rev. Lett.* **109**, 095301 (2012).
- [9] M. Atala, M. Aidelsburger, J. T. Barreiro, D. Abanin, T. Kitagawa, E. Demler, and I. Bloch, *Nature Phys.* **9**, 795 (2013).
- [10] M. Aidelsburger, M. Atala, M. Lohse, J. T. Barreiro, B. Paredes, and I. Bloch, *Phys. Rev. Lett.* **111**, 185301 (2013).
- [11] H. Miyake et al., *Phys. Rev. Lett.* **111**, 185302 (2013).

- [12] C. J. Kennedy et al., Phys. Rev. Lett. **111**, 225301 (2013)
- [13] M. Atala et al., arXiv:1402.0819 (2014).
- [14] D.C. Tsui, H.L. Stormer, and A.C. Gossard, Phys. Rev. Lett. **48**, 1559 (1982).
- [15] T.D. Stanescu, B. Anderson, and V. Galitski, Phys. Rev. A **78**, 023616 (2008); C. Wang, C. Gao, C.-M. Jian, and H. Zhai, Phys. Rev. Lett **105**, 160403 (2010); T.-L. Ho and S. Zhang, Phys. Rev. Lett. **107**, 150403 (2011); J. Radic, T. A. Sedrakyan, I. B. Spielman, and V. Galitski, Phys. Rev. A **84**, 063604 (2011); C. Wu, I. M. Shem, and X.-F. Zhou, Chin. Phys. Lett. **28**, 097102 (2011); Y. Li, L. P. Pitaevskii, and S. Stringari, Phys. Rev. Lett. **108**, 225301 (2012); T. A. Sedrakyan, A. Kamenev, and L. I. Glazman, Phys. Rev. A **86**, 063639 (2012); Y. Zhang, L. Mao, and C. Zhang, Phys. Rev. A **108**, 035302 (2012); T. Ozawa and G. Baym, Phys. Rev. A **85**, 013612 (2012) and Phys. Rev. Lett. **110**, 085304 (2013), X.-F. Zhou, Y. Li, Z. Cai, C. Wu, J. Phys. B: At. Mol. Opt. Phys. **46** 134001 (2013).
- [16] T. Graß, K. Saha, K. Sengupta, and M. Lewenstein, Phys. Rev. A **84**, 053632 (2011).
- [17] W. S. Cole, S. Zhang, A. Paramekanti, and N. Trivedi, Phys. Rev. Lett. **109**, 085302 (2012).
- [18] J. Radic, A. Di Ciolo, K. Sun, and V. Galitski, Phys. Rev. Lett. **109**, 085303 (2012).
- [19] Z. Cai, X. Zhou, and C. Wu, Phys. Rev. A **85**, 061605(R) (2012).
- [20] S. Mandal, K. Saha, and K. Sengupta, Phys. Rev. B **86**, 155101 (2012).
- [21] C. H. Wong and R. A. Duine, Phys. Rev. Lett. **110**, 115301 (2013).
- [22] Y. Qian, M. Gong, V. W. Scarola, and C. Zhang, arXiv:1312.4011
- [23] D.-W. Zhang, J.-P. Chen, C.-J. Shan, Z. D. Wang, and S.-L. Zhu, Phys. Rev. A **88**, 013612 (2013).
- [24] T. Graß, B. Juliá-Díaz, N. Barberán, and M. Lewenstein, Phys. Rev. A **86**, 021603(R) (2012)
- [25] T. Graß, B. Juliá Díaz, M. Burrello, and M. Lewenstein, J. Phys. B: At. Mol. Opt. Phys. **46**, 134006 (2013).
- [26] I. Dzyaloshinsky, J. Phys. Chem. Solids **4**, 241 (1958).
- [27] T. Moriya, Phys. Rev. **120**, 91 (1960).
- [28] U. Schollwöck, Ann. Phys. **326**, 96 (2011).
- [29] G. De Chiara, M. Rizzi, D. Rossini, and S. Montangero, J. Comput. Theor. Nanosci. **5**, 1277 (2008).
- [30] J. Alicea, Rep. Prog. Phys. **75**, 076501 (2012).
- [31] C. W. J. Beenakker, Annu. Rev. Con. Mat. Phys. **4**, 113 (2013).
- [32] A. Y. Kitaev, Phys. Usp. **44**, 131 (2001).
- [33] S. Gangadharaiah, B. Braunecker, P. Simon, and D. Loss, Phys. Rev. Lett. **107**, 036801 (2011).
- [34] E. M. Stoudenmire, J. Alicea, O.A. Starykh, and M.P. Fisher, Phys. Rev. **84**, 014503 (2011).
- [35] A. M. Lobos, R. M. Lutchyn, and S. Das Sarma, Phys. Rev. Lett. **109**, 146403 (2012).
- [36] B. Braunecker and P. Simon, Phys. Rev. Lett. **111**, 147202 (2013).
- [37] R. J. Baxter, *Exactly solved models in statistical mechanics* (Academic Press, 1989).
- [38] E. Ercolessi, S. Evangelisti, F. Franchini, and F. Ravanini, Phys. Rev. B **88**, 104418 (2013).
- [39] V.M. Kontorovich and V.M. Tsukernik, Zh. Eksp. Teor. Fiz. **52** 1446 (1967) [Sov. Phys. JETP **25** 960 (1967)].
- [40] Th.J. Siskens, H.W. Capel and K.J.F. Gaemers, Physica A **79** 259 (1975).
- [41] Th.J. Siskens and H.W. Capel, Physica A **79** 296 (1975).
- [42] J.H.H. Perk and H.W. Capel, Phys. Lett. A **58** 115 (1976).
- [43] V. E. Korepin, *Quantum Inverse Scattering Method and Correlation Functions* (Cambridge University Press, 1997).
- [44] M. Campostrini, A. Pelissetto and E. Vicari, Phys. Rev. B **89**, 094516 (2014).
arXiv:1401.0788, Phys. Rev. B (2014) in press.
- [45] M. E. Fisher, M. N. Barber, and D. Jasnow, Phys. Rev. A **8**, 1111 (1973).
- [46] A. Pelissetto and E. Vicari, Phys. Rep. **368**, 549 (2002).
- [47] G. Ceccarelli, C. Torrero, and E. Vicari, Phys. Rev. B **87**, 024513 (2013).
- [48] L.-M. Duan, E. Demler, and M. D. Lukin, Phys. Rev. Lett. **91**, 090402 (2003).
- [49] G. Sun, J. Jaramillo, L. Santos, and T. Vekua, Phys. Rev. B **88**, 165101 (2013).

- [50] J. Zhao, S. Hu, J. Chang, F. Zheng, P. Zhang, and X. Wang, arXiv:1403.1316 (2014).
- [51] M. Piraud, Z. Cai, I. P. McCulloch, and U. Schollwöck, arXiv:1403.3350 (2014).
- [52] Z. Xu, W. Cole, and S. Zhang, arXiv:1403.3491 (2014).